Evaporation of binary-mixture liquid droplets: picoliter pancakes

Amir A. Pahlavan,[1,*] Lisong Yang,[2,*] Colin D. Bain,[2] and Howard A. Stone[1,†]

[1] *Department of Mechanical and Aerospace Engineering, Princeton University, NJ 08544, USA*
[2] *Department of Chemistry, Durham University, Durham, DH1 3LE, UK*

Small multicomponent droplets are of increasing importance in a plethora of technological applications ranging from the fabrication of self-assembled hierarchical patterns to the design of autonomous fluidic systems. While often far away from equilibrium, involving complex and even chaotic flow fields, it is commonly assumed that in these systems with small drops surface tension keeps the shapes spherical. Here, studying picoliter volatile binary-mixture droplets of isopropanol and 2-butanol, we show that the dominance of surface tension forces at small scales can play a dual role: minute variations in surface tension along the interface can create Marangoni flows that are strong enough to significantly deform the drop, forming micron-thick pancake-like shapes that are otherwise typical of large puddles. We identify the conditions under which these flattened shapes form and explain why, universally, they relax back to a spherical-cap shape towards the end of drop lifetime. We further show that the formation of pancake-like droplets suppresses the "coffee-ring" effect and leads to uniform deposition of suspended particles. The quantitative agreement between theory and experiment provides a predictive capability to modulate the shape of tiny droplets with implications in a range of technologies from fabrication of miniature optical lenses to coating, printing and pattern deposition.

Surface tension gives small droplets their spherical shape to minimize the interfacial energy at equilibrium [1, 2]. Away from equilibrium, however, the drop shape becomes coupled to the mass and energy transfer in the bulk of the fluids on the two sides and across the interface, and one might therefore expect the drop to become deformed. Despite this expectation, with few exceptions [3–7], the general consensus has been that as the drop size decreases surface tension becomes the dominant force, retaining a spherical shape even far from equilibrium [8–16]. In this work, we show that this intuitive argument breaks down in multicomponent drops.

When a wetting nonvolatile liquid drop is deposited on a solid substrate, it spreads to form a molecularly-thin film [2]. A wetting volatile liquid, however, loses mass via evaporation as it spreads, and starts shrinking at some time while keeping a spherical-cap shape during its entire evolution (Fig. 1(a)) [17, 18]. A wetting volatile binary-mixture drop, i.e., one with two components might be expected to show a behavior intermediate of its constituents. It has been shown that solutal Marangoni flows can enhance or inhibit the spreading [19–21], leading to deviations from spherical-cap shapes in microliter multicomponent drops [3, 5, 6, 22], where the influence of gravity cannot be ruled out a priori [14, 15]. However, it remains unclear whether such shape deviations can be observed at smaller scales, where surface tension forces dominate. Here, combining experiments and theoretical modeling, we report on the observation that picoliter volatile binary-mixture droplets, for which gravitational effects are negligible, can strongly deviate from the spherical-cap shape and even become completely flattened as they evaporate (Fig. 1(a)). We discuss the role of differential evaporation of the components and the resulting solutal Marangoni flow in the modulation of the shape of the evaporating droplets, identifying the critical criterion for transition from a spherical-cap to a pancake-like shape.

We deposit picoliter-size ($20-50$ pL) droplets of pure isopropanol (IPA) and 2-butanol, and their binary mixture on glass substrates (see the Supplementary Material [23]). IPA–2-butanol mixture is zeotropic and thermodynamically close to ideal [24]. The vapor pressure of IPA is nearly twice that of 2-butanol. The differential evaporation of the components together with the fact that the evaporative flux in thin drops diverges towards the edge of the drop [25, 26] leads to the depletion of the more volatile component near the edge [5, 6, 27]. The initially uniform and well-mixed binary drop therefore develops spatial gradients in composition, which further creates interfacial gradients in the surface tension, and the vapor saturation concentration of the two components, and in turn modifies their evaporative fluxes (Fig. 1(b)).

A model for the evaporation of binary drops needs to account for the coupling between the flow field within the drop, the shape of the drop, and the vapor concentration field above the drop [6, 12]. The flow within the drop is described using the lubrication approximation given that the height of the droplets $h_0 \approx 1$ μm is much smaller than their radius $R \approx 50$ μm, i.e., $h_0/R \ll 1$, and inertial effects are negligible compared to the viscous effects, i.e., the Reynolds number is small, where $\mathrm{Re} = \rho U h_0 (h_0/R)/\mu \approx 10^{-4} \ll 1$, with $U = \mathrm{O}(1)$ mm/s as the characteristic liquid velocity and $\mu \approx 2$ mPa.s and $\rho \approx 800$ kg/m^3 as the liquid viscosity and density, respectively. The timescale of diffusion of the components across the height of the drop scales as $h_0^2/D_l \approx 1$ ms, where the liquid diffusivity $D_l \approx 10^{-9}$ m^2/s. This diffusion timescale is much smaller than the evaporative timescale of the drop $h_0/(J_{\mathrm{ave}}/\rho) \approx 25$ ms, where J_{ave} is

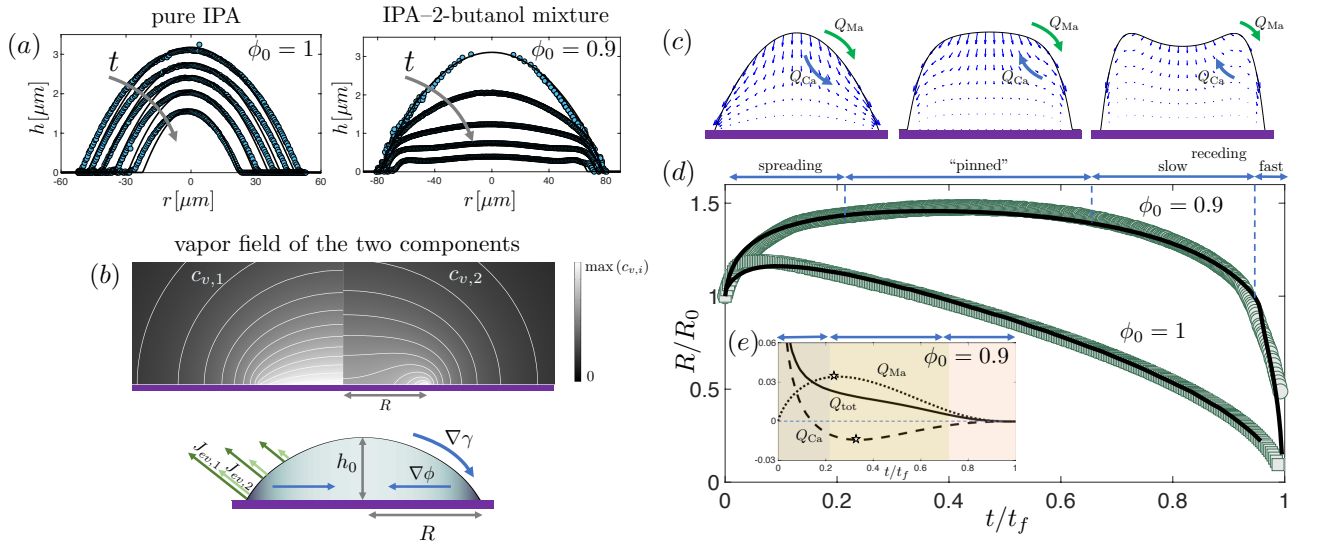

FIG. 1. Binary-mixture droplets become flattened, forming micron-thick pancake-like shapes as they evaporate. (a) While a pure IPA droplet ($\phi_0 = 1$) keeps a spherical-cap shape during its entire evolution, a binary-mixture droplet of 90% IPA and 10% 2-butanol ($\phi_0 = 0.9$) becomes completely flattened, forming a micron-thick pancake-like shape. (b) The two components in the mixture evaporate at different rates. This differential evaporation creates a spatial gradient in the volume fractions ϕ within the drop that affects the vapor fields of the two components, $c_{v,1}$ and $c_{v,2}$, and therefore their evaporative fluxes, $J_{ev,1}$ and $J_{ev,2}$. (c) The differential evaporation of the two components creates a solutal Marangoni flow, $Q_{\rm Ma} = \int_0^R h\bar{u}_{\rm Ma} 2\pi r dr$, along the interface from the apex to the edge of the drop that (d) leads to an enhanced spreading at early times, where $R(t)$ is the drop radius. (e) This Marangoni flow flattens the drop in the middle and enhances the curvature near the edge, creating an opposing capillary flow, $Q_{\rm Ca} = \int_0^R h\bar{u}_{\rm Ca} 2\pi r dr$, at intermediate times. The solutal Marangoni flow replenishes the edge with fresh fluid and keeps the edge from receding, effectively "pinning" the drop for a substantial part of its lifetime. At late times, the solutal Marangoni flow weakens and the drop starts to recede. In stark contrast, a pure IPA droplet ($\phi_0 = 1$) rapidly switches from spreading to receding as it evaporates. The simulations in (b) and (c) correspond to $\phi_0 = 0.9$. The symbols in (a) and (d) represent experimental data and the lines represent the simulations.

the average evaporative flux for a pure IPA droplet, indicating the components are well-mixed across the height of the drop (see the Supplementary Material).

Therefore, the coupled evolution of the height of the drop $h(r,t)$, and the volume fractions $\phi_i(r,t)$ with $i = 1, 2$ representing the two volatile components, are describe by

$$\frac{\partial h}{\partial t} = \underbrace{-\frac{1}{r}\frac{\partial}{\partial r}\left(rh\bar{u}\right)}_{\text{fluid flow}} - \underbrace{J_{ev,t}}_{\text{evaporation}}, \tag{1}$$

$$\frac{\partial\left(h\phi_1\right)}{\partial t} = \underbrace{\frac{1}{r}\frac{\partial}{\partial r}\left(rhD_l\frac{\partial\phi_1}{\partial r}\right)}_{\text{diffusion}} - \underbrace{\frac{1}{r}\frac{\partial}{\partial r}\left(rh\bar{u}\phi_1\right)}_{\text{convection}} - \underbrace{J_{ev,1}}_{\text{evaporation}} \tag{2}$$

in which $J_{ev,t} = J_{ev,1} + J_{ev,2}$ is the total evaporative flux, and $J_{ev,i}$ are the evaporative fluxes of the two components. The height-averaged velocity is defined as

$$\bar{u}(r,t) = \underbrace{\frac{h^2}{3\mu}\frac{\partial p}{\partial r}}_{\bar{u}_{\rm Ca}\text{:capillary flow}} + \underbrace{\frac{h}{2\mu}\frac{d\gamma}{d\phi_1}\frac{\partial\phi_1}{\partial r}}_{\bar{u}_{\rm Ma}\text{:solutal Marangoni flow}}, \tag{3}$$

where the liquid pressure $p = \gamma\kappa + \Pi(h)$ with $\Pi(h) = A/h^3$ as the disjoining pressure, $A \approx 10^{-20}$ J as the Hamaker constant, and the curvature $\kappa = -\nabla^2 h$. We denote $\phi \equiv \phi_1$ as the volume fraction of the more volatile IPA, and the volume fraction of the 2-butanol is $\phi_2 = 1-\phi$. The second term in Eq. (3) represents the contribution of the solutal Marangoni flow due to gradients in the surface tension $\gamma(r,t)$, where $d\gamma/d\phi = -1.6$ mN/m for the IPA–2-butanol mixture, assuming a linear dependence of surface tension on the volume fraction.

The characteristic timescale of vapor diffusion $\tau_D = R^2/D_v \approx 1$ ms, where $D_v \approx 10^{-5}$ m^2/s is the vapor diffusion coefficient, is much smaller than the timescale of drop evaporation $t_f \approx 100$ ms. Thus, we model the vapor field as diffusion-limited and quasi-steady: $\nabla^2 c_{v,i} = 0$, where $c_{v,i}$ are the vapor concentrations of the two components $i = 1, 2$. A thin drop can be approximated as a disk with zero height [25, 26]. According to Raoult's law for an ideal mixture the vapor concentration on the interface of the drop is proportional to the saturation concentration $c_{v,i} = x_i c_{s,i}$ with x_i as the liquid mole fraction, which given that both liquids have a similar density can be written as $x_i = (\phi_i/M_i)\,/\,[\phi/M_1 + (1-\phi)/M_2]$, where M_i are the molecular weights of the two components. We consider the concentration of the two components to be zero far away from the drop $c_{v,i}|_{r\to\infty} = 0$. The evaporative fluxes are $J_{ev,i} = -(D_v/\rho)\mathbf{n}\cdot\nabla c_{v,i}$, where $\mathbf{n}$ is the unit normal vector directed away from the liquid phase.

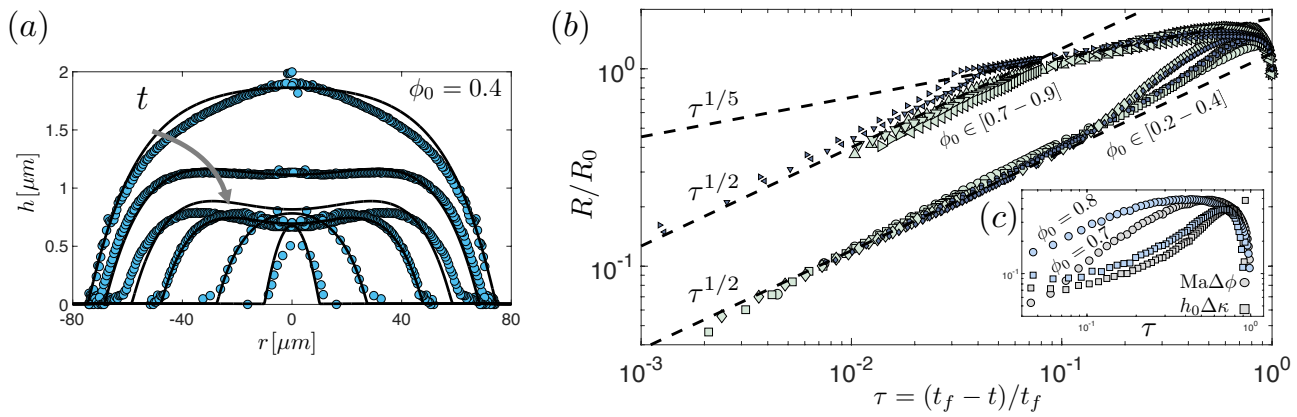

FIG. 2. (a) The flattened binary-mixture droplets relax to a spherical-cap shape towards the end of their lifetime when the solutal Marangoni flows become sufficiently weak. (b) The radius of binary drops with low initial volume fractions follows the scaling $R \sim \tau^{1/2}$. The radius of drops with high initial volume fractions, however, deviates strongly from this behavior at intermediate times and can be described by $R \sim \tau^{1/5}$ before crossing over to the $R \sim \tau^{1/2}$ scaling at late times (smaller τ). (c) The crossover between the two scaling regimes signals the transition from a flattened shape to a spherical-cap shape and occurs when the solutal Marangoni-driven flow, which is proportional to $\mathrm{Ma}\Delta\phi$ becomes weaker than the opposing capillary-driven flow, which is proportional to $h_0\Delta\kappa$. In (b), the larger symbols represent the experimental data and the smaller symbols represent the corresponding simulation.

This coupled model is compared below to experiments, and allows us to monitor the evolution of the composition field within the drop and isolate the Marangoni and capillary contributions to the flow field and drop shape (see the Supplementary Material).

The simulations show that the solutal Marangoni flow moves the liquid from the center of the drop to the edge, flattening the drop in the middle and enhancing the curvature near the edge, therefore creating an opposing capillary flow from the edge towards the middle (Fig. 1(c, e)). As long as the solutal Marangoni flow remains strong enough to overcome this opposing capillary flow, the pancake shape persists. Although the contact line is free to move, it remains nearly "pinned" for a significant part of the lifetime of the drop. As the evaporation continues removing the more volatile phase, the drop runs out of fuel, i.e., the composition gradient along the drop weakens and the drop recedes (Fig. 1(d, e); see also Fig. 3 of the Supplementary Material). The experimental measurements of the droplet profile and radius (symbols) are in good agreement with the simulations (lines) as shown in Fig. 1.

As the drop begins to recede, the capillary flow overcomes the solutal Marangoni flow and relaxes the drop back to a spherical-cap shape (Fig. 2(a)). A qualitatively similar observation has been reported in microliter multicomponent drops [3]. This relaxation is accompanied by a crossover in the scaling of the radius of the drop with time as shown by both experiments and simulations (Fig. 2(b)). In the case of pure liquids with spherical-cap shape (Fig. 1(a)), the integrated evaporative flux of the drop scales with its radius [25, 26] and conservation of mass leads to $dV/d\tau \sim R$, where $\tau = (t_f - t)/t_f$ and t_f represents the drop lifetime. The volume of a spherical-cap drop scales with its radius as $V \sim R^3$ and together with conservation of mass leads to the $R \sim \tau^{1/2}$ scaling of radius with time known as the "d^2 law" [17, 28]. We observe that at low initial volume fractions ϕ_0 of the more volatile phase, as the drop recedes its radius follows the $R \sim \tau^{1/2}$ scaling for most of its lifetime (Fig. 2(b)). For high ϕ_0 values, however, we observe that the radius of the drop follows a different path in time and the results collapse on a different curve: the drop radius first follows a scaling with time, $R \sim \tau^{1/5}$, before crossing over to the familiar $R \sim \tau^{1/2}$ scaling at late times (Fig. 2(b)) (also see Figs. 4 and 5 of the Supplementary Material). The underlying reason for the observation of the $R \sim \tau^{1/5}$ scaling regime remains to be investigated.

This crossover from the pancake to the spherical-cap regime can be understood in terms of a competition between the solutal Marangoni flow and the opposing capillary flow (Fig. 1(c)). In the lubrication model (Eq. (3)), the capillary term scales as $(\gamma/\mu)(h_0/R)^3$ and the solutal Marangoni term scales as $(\Delta\gamma/\mu)(h_0/R)$. The surface tension variation $\Delta\gamma$ is due to the compositional gradient $\Delta\phi$ along the interface created by the differential evaporation of the two components: $\Delta\gamma = |d\gamma/d\phi|\,\Delta\phi$. The necessary condition to produce drop deformation is to have the Marangoni flow dominate the capillary flow, i.e.,

$$\Delta\phi \gtrsim \left(\frac{\gamma}{|d\gamma/d\phi|}\right)\left(\frac{h_0}{R}\right)^2 \equiv \Delta\phi_{cr}, \tag{4}$$

which shows that the compositional gradient along the interface needs to be stronger than a critical magnitude for a pancake to form. This scaling argument is supported by our numerical simulations of the coupled

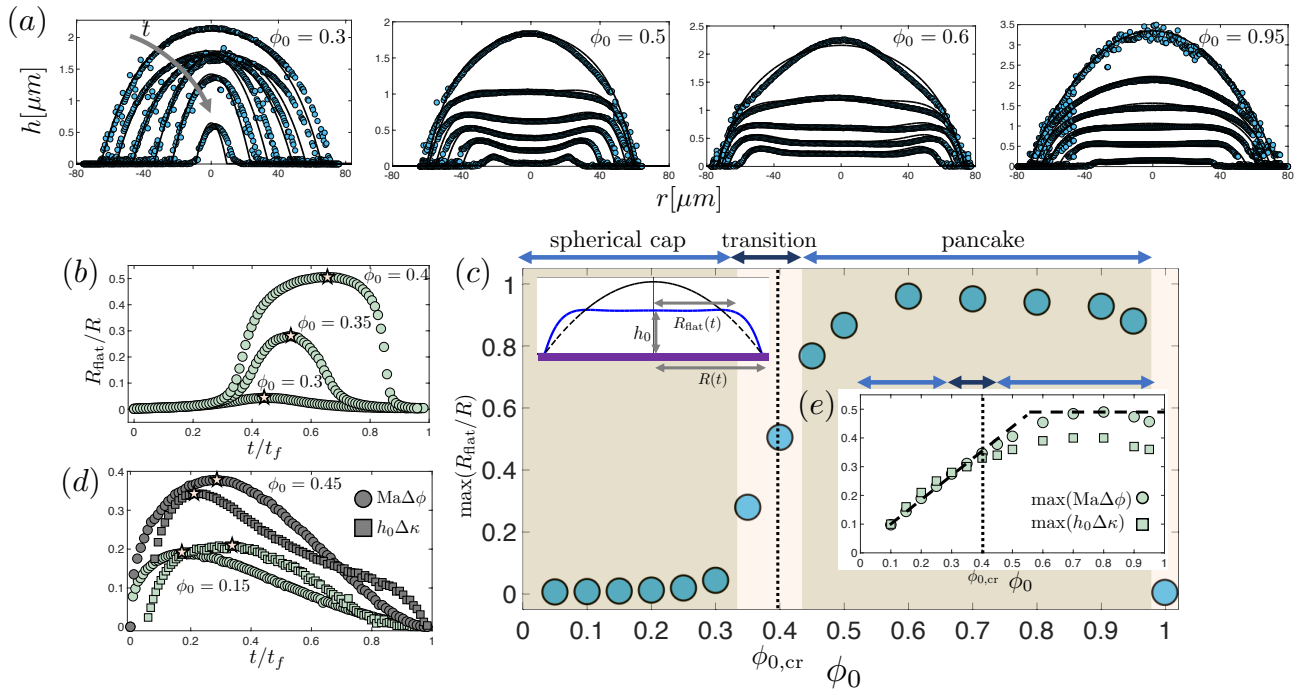

FIG. 3. (a) The flattened pancake-like shapes only form when the initial volume fraction of the more volatile component exceeds a critical value $\phi_0 > \phi_{0,\mathrm{cr}} \approx 0.4$. The symbols and lines represent experiments and simulations, respectively. (b) The transition from the spherical-cap regime at low ϕ_0 to the pancake regime at high ϕ_0 can be quantified by monitoring the evolution of the ratio of the radius of the flattened part of the drop, R_{flat} (inset of (c)), to the radius of the drop R, i.e., R_{flat}/R. This ratio reaches a maximum value before decaying to zero as the drop relaxes to a spherical-cap shape. (c) This maximum value, $\max(R_{\mathrm{flat}}/R)$, shows a sharp transition from ≈ 0 at low volume fractions corresponding to the spherical-cap regime, to ≈ 1 when $\phi_0 > \phi_{0,\mathrm{cr}}$ corresponding to the pancake regime, which persists almost all the way to $\phi_0 \approx 1$. (d) Simulations (symbols) show that the compositional gradient $\mathrm{Ma}\Delta\phi$ within the drop reaches a peak during the evaporation and then decays to zero. (e) The peak composition gradient increases almost linearly with ϕ_0, and when stronger than a critical value $\Delta\phi > \Delta\phi_{cr}$ (Eq. (4)), corresponding to the constraint $\phi_0 > \phi_{0,cr} \approx 0.4$ (Eq. (5)), leads to the formation of a pancake shape.

model, which show that the crossover from the pancake to the spherical-cap regime occurs when the solutal Marangoni flow, which is proportional to $\mathrm{Ma}\Delta\phi$ becomes weaker than the opposing capillary flow, which is proportional to $(4/\theta_0^2)h_0\Delta\kappa$ (Fig. 2(c)). This balance translates to the criterion $\Delta\phi < (2/3)\,(\gamma_0/\,|d\gamma/d\phi|)\,h_0\Delta\kappa$, which is equivalent to Eq. (4) if we take the variation in curvature $\Delta\kappa \approx h_0/R^2$. Here, the Marangoni number is defined as $\mathrm{Ma} = -(6/\theta_0^2)(d\gamma/d\phi)/\gamma_0$ with θ_0 as the initial contact angle of the deposited drop, and γ_0 as the surface tension of IPA (see the Supplementary Material).

The presence of the two distinct temporal responses in Fig. 2(b) is suggestive of a transition as the initial volume fraction increases beyond a critical value, i.e., when $\phi_0 > \phi_{0,cr}$. Indeed, we observe a transition from the spherical-cap regime at low initial volume fractions $\phi_0 < \phi_{0,cr}$, where deviations from the spherical-cap shape are minimal, to the pancake regime at high initial volume fractions $\phi_0 > \phi_{0,cr}$, where the drops become completely flattened for a substantial part of their lifetime (Fig. 3(a)).

The extent of the nearly flat shape of the drop relative to the radius of the drop R_{flat}/R provides a quantitative measure of the deviation from the spherical-cap shape (inset of Fig. 3(c)). We define the flat region as the part with absolute value of the slope less than $\theta_0/100$. This ratio starts from zero when a well-mixed spherical binary drop is deposited on the substrate, increases in time to reach a maximum value as the drop deforms, and then decays to zero as the drop relaxes to a spherical-cap shape towards the end of its lifetime (Fig. 3(b)). The maximum value of R_{flat}/R therefore serves as a measure of the maximum deviation from a spherical cap. Consistent with the transition between the two temporal responses observed in Fig. 2(b) as the initial volume fraction increases, we observe that at low volume fractions $\max(R_{\mathrm{flat}}/R)$ is close to zero, while beyond a critical initial volume fraction it sharply increases and remains close to 1 before sharply returning to zero for a pure (single-component) IPA drop with $\phi_0 = 1$ (Fig. 3(c)).

The transition from the spherical-cap to the pancake regime as the initial volume fraction increases beyond a critical value $\phi_{0,cr}$ (Fig. 3(c)) can be understood based on the arguments leading to Eq. (4), which show that the compositional gradient within the drop needs to be strong enough for a pancake shape to form, i.e., $\Delta\phi \gtrsim$

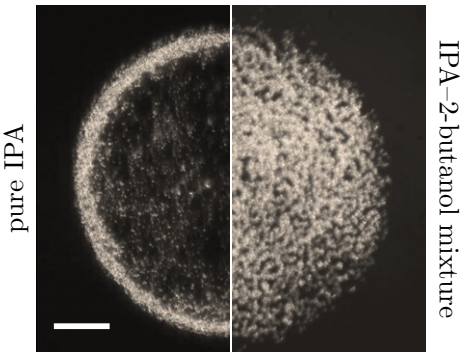

FIG. 4. The "coffee-ring" effect becomes suppressed, leaving a uniform deposit in the binary-mixture drop. The deposits of poly(N-vinylpyrrolidone)-stabilized polystyrene particles (755 nm) from pure IPA droplet (left) and IPA–2-butanol droplet with $\phi_0 = 0.9$ (right). The scalebar is 30 μm.

$\Delta\phi_{cr}$. Our simulations show that the peak strength of the solutal Marangoni flow, which scales as $\mathrm{Ma}\Delta\phi$, increases almost linearly with ϕ_0, i.e., $\max(\mathrm{Ma}\Delta\phi) \sim \phi_0$, before saturating to a nearly constant value $\Delta\phi \approx 0.15$ corresponding to $\Delta\gamma \approx 0.2$ mN/m, at high initial volume fractions (Fig. 3(d,e)). Therefore, the critical compositional gradient constraint in Eq. (4) translates to a constraint on the critical initial volume fraction for the transition from the spherical-cap to the pancake regime:

$$\phi_0 \gtrsim \phi_{0,cr}, \tag{5}$$

where our experiments and theoretical model show that $\phi_{0,cr} \approx 0.4$ for the IPA–2-butanol mixture (Fig. 3(e)). Therefore, we can modulate the drop shape by varying the initial volume fraction of the more volatile component. The control over the shape of the picoliter droplets can be utilized to fabricate micro/nano lenses [29–31] with applications in imaging [32], biosensing [33], and 3D displays [34].

In coating technologies, one of the main challenges has been to achieve a uniform deposition pattern due to the "coffee ring" effect that concentrates the particles at the edge of the evaporating droplet [11, 25, 35–41]. It has recently been shown that flattened binary-mixture droplets can suppress the "coffee ring" effect and form uniform 2D-crystal patterns [7]. Our work shows that the binary-mixture droplets can remain nearly "pinned" and flattened over a substantial part of their lifetime. This geometric effect together with the internal flow due to solutal Marangoni and capillary forces provides a plausible mechanism for the suppression of the "coffee ring" effect in a picoliter pancake (Fig. 4; see also Supplementary Movies 3 and 4). To go beyond this description, the particle dynamics in the mixture and their effect on the contact line motion need to be accounted for in the simulations [42–46].

Our study provides a predictive capacity for formulators of solvent-based inks to exploit (or avoid) Marangoni effects in coating and printing applications [47]. While here we focused on the IPA–2-butanol mixture, we have observed the formation of pancake-shaped droplets in a variety of binary-liquid pairs that satisfy the appropriate criteria on the relative surface tensions and volatilities. A more extensive study of the parameter space spanned by different binary liquids will be presented in the future. It would be interesting to further explore the evaporation dynamics in the presence of surface roughness, different surface wetting conditions, spatiotemporal variations in the rheological properties of the mixtures, and phase separation [2, 12, 47–55]. We anticipate our observations will have implications for many technological applications involving multicomponent drops [16, 35, 56–58], where minute variation in surface tension due to nonuniform compositions within the drops can lead to strong flows and shape deformations.

ACKNOWLEDGMENTS

A.A. Pahlavan and H.A. Stone acknowledge funding from ExxonMobil Research and the Andlinger Center for Energy and the Environment at Princeton. L. Yang and C.D. Bain acknowledge funding from the Engineering and Physical Sciences Research Council under grant EP/N025245/1. The raw experimental data that are associated with the data in the figures are available through the University of Durham data repository: doi:10.15128/r1bk1289931.

* These authors have contributed equally to this work.
† hastone@princeton.edu

[1] J. S. Rowlinson and B. Widom, *Molecular Theory of Capillarity* (Courier Corporation, 2013).
[2] P. G. de Gennes, Wetting: statics and dynamics, Rev. Mod. Phys. **57**, 827 (1985).
[3] G. Guéna, C. Poulard, and A. Cazabat, Evaporating drops of alkane mixtures, Colloids and Surfaces A: Physicochemical and Engineering Aspects **298**, 2 (2007).
[4] Y. Tsoumpas, S. Dehaeck, A. Rednikov, and P. Colinet, Effect of Marangoni flows on the shape of thin sessile droplets evaporating into air, Langmuir **31**, 13334 (2015).
[5] S. Karpitschka, F. Liebig, and H. Riegler, Marangoni contraction of evaporating sessile droplets of binary mixtures, Langmuir **33**, 4682 (2017).
[6] C. Diddens, H. Tan, P. Lv, M. Versluis, J. G. M. Kuerten, X. Zhang, and D. Lohse, Evaporating pure, binary and ternary droplets: thermal effects and axial symmetry breaking, Journal of Fluid Mechanics **823**, 470 (2017).
[7] G. Hu, L. Yang, Z. Yang, Y. Wang, X. Jin, J. Dai, Q. Wu, S. Liu, X. Zhu, X. Wang, T.-C. Wu, R. C. T. Howe, T. Albrow-Owen, L. W. T. Ng, Q. Yang, L. G. Occhipinti, R. I. Woodward, E. J. R. Kelleher, Z. Sun, X. Huang, M. Zhang, C. D. Bain, and T. Hasan, A general ink for-

mulation of 2d crystals for wafer-scale inkjet printing, Science Advances **6** (2020).
[8] J. R. E. Christy, Y. Hamamoto, and K. Sefiane, Flow transition within an evaporating binary mixture sessile drop, Phys. Rev. Lett. **106**, 205701 (2011).
[9] R. Bennacer and K. Sefiane, Vortices, dissipation and flow transition in volatile binary drops, Journal of Fluid Mechanics **749**, 649 (2014).
[10] S. Shin, I. Jacobi, and H. A. Stone, Bénard–Marangoni instability driven by moisture absorption, EPL (Europhysics Letters) **113**, 24002 (2016).
[11] H. Kim, F. Boulogne, E. Um, I. Jacobi, E. Button, and H. A. Stone, Controlled uniform coating from the interplay of Marangoni flows and surface-adsorbed macromolecules, Phys. Rev. Lett. **116**, 124501 (2016).
[12] H. Tan, C. Diddens, P. Lv, J. G. M. Kuerten, X. Zhang, and D. Lohse, Evaporation-triggered microdroplet nucleation and the four life phases of an evaporating ouzo drop, Proceedings of the National Academy of Sciences **113**, 8642 (2016).
[13] P. J. Sáenz, A. W. Wray, Z. Che, O. K. Matar, P. Valluri, J. Kim, and K. Sefiane, Dynamics and universal scaling law in geometrically-controlled sessile drop evaporation, Nature Communications **8**, 14783 (2017).
[14] A. M. J. Edwards, P. S. Atkinson, C. S. Cheung, H. Liang, D. J. Fairhurst, and F. F. Ouali, Density-driven flows in evaporating binary liquid droplets, Phys. Rev. Lett. **121**, 184501 (2018).
[15] Y. Li, C. Diddens, P. Lv, H. Wijshoff, M. Versluis, and D. Lohse, Gravitational effect in evaporating binary microdroplets, Phys. Rev. Lett. **122**, 114501 (2019).
[16] D. Lohse and X. Zhang, Physicochemical hydrodynamics of droplets out of equilibrium, Nature Reviews Physics **2**, 426 (2020).
[17] A.-M. Cazabat and G. Guéna, Evaporation of macroscopic sessile droplets, Soft Matter **6**, 2591 (2010).
[18] E. Jambon-Puillet, O. Carrier, N. Shahidzadeh, D. Brutin, J. Eggers, and D. Bonn, Spreading dynamics and contact angle of completely wetting volatile drops, Journal of Fluid Mechanics **844**, 817 (2018).
[19] D. Pesach and A. Marmur, Marangoni effects in the spreading of liquid mixtures on a solid, Langmuir **3**, 519 (1987).
[20] A. G. L. Williams, G. Karapetsas, D. Mamalis, K. Sefiane, O. K. Matar, and P. Valluri, Spreading and retraction dynamics of sessile evaporating droplets comprising volatile binary mixtures, Journal of Fluid Mechanics **907**, A22 (2021).
[21] M. Abo Jabal, E. Homede, A. Zigelman, and O. Manor, Coupling between wetting dynamics, marangoni vortices, and localized hot cells in drops of volatile binary solutions, Journal of Colloid and Interface Science **588**, 571 (2021).
[22] C. Diddens, J. Kuerten, C. van der Geld, and H. Wijshoff, Modeling the evaporation of sessile multi-component droplets, Journal of Colloid and Interface Science **487**, 426 (2017).
[23] See Supplemental Material [url] for the details of the experimental protocol and theoretical model, which includes Refs. [59-73].
[24] A. Tamir and J. Wisniak, Vapor-liquid equilibriums of isobutanol-n-butanol and isopropanol-sec-butanol systems, Journal of Chemical & Engineering Data **20**, 391 (1975).
[25] R. D. Deegan, O. Bakajin, T. F. Dupont, G. Huber, S. R. Nagel, and T. A. Witten, Capillary flow as the cause of ring stains from dried liquid drops, Nature **389**, 827 (1997).
[26] H. Hu and R. G. Larson, Evaporation of a sessile droplet on a substrate, The Journal of Physical Chemistry B **106**, 1334 (2002).
[27] H. Kim and H. A. Stone, Direct measurement of selective evaporation of binary mixture droplets by dissolving materials, Journal of Fluid Mechanics **850**, 769 (2018).
[28] R. G. Larson, Transport and deposition patterns in drying sessile droplets, AIChE Journal **60**, 1538 (2014).
[29] L. Dong, A. K. Agarwal, D. J. Beebe, and H. Jiang, Adaptive liquid microlenses activated by stimuli-responsive hydrogels, Nature **442**, 551 (2006).
[30] X. Zhang, J. Ren, H. Yang, Y. He, J. Tan, and G. G. Qiao, From transient nanodroplets to permanent nanolenses, Soft Matter **8**, 4314 (2012).
[31] S. Nagelberg, L. D. Zarzar, N. Nicolas, K. Subramanian, J. A. Kalow, V. Sresht, D. Blankschtein, G. Barbastathis, M. Kreysing, T. M. Swager, and M. Kolle, Reconfigurable and responsive droplet-based compound microlenses, Nature Communications **8**, 14673 (2017).
[32] N.-T. Nguyen, Micro-optofluidic lenses: A review, Biomicrofluidics **4**, 031501 (2010).
[33] S. M. Borisov and O. S. Wolfbeis, Optical biosensors, Chemical Reviews **108**, 423 (2008).
[34] X. Xiao, B. Javidi, M. Martinez-Corral, and A. Stern, Advances in three-dimensional integral imaging: sensing, display, and applications, Appl. Opt. **52**, 546 (2013).
[35] J. Park and J. Moon, Control of colloidal particle deposit patterns within picoliter droplets ejected by ink-jet printing, Langmuir **22**, 3506 (2006).
[36] P. J. Yunker, T. Still, M. A. Lohr, and A. G. Yodh, Suppression of the coffee-ring effect by shape-dependent capillary interactions, Nature **476**, 308 (2011).
[37] T. Still, P. J. Yunker, and A. G. Yodh, Surfactant-induced Marangoni eddies alter the coffee-rings of evaporating colloidal drops, Langmuir **28**, 4984 (2012).
[38] M. Majumder, C. S. Rendall, J. A. Eukel, J. Y. L. Wang, N. Behabtu, C. L. Pint, T.-Y. Liu, A. W. Orbaek, F. Mirri, J. Nam, A. R. Barron, R. H. Hauge, H. K. Schmidt, and M. Pasquali, Overcoming the "coffee-stain" effect by compositional Marangoni-flow-assisted drop-drying, The Journal of Physical Chemistry B **116**, 6536 (2012).
[39] E. L. Talbot, H. N. Yow, L. Yang, A. Berson, S. R. Biggs, and C. D. Bain, Printing small dots from large drops, ACS Applied Materials & Interfaces **7**, 3782 (2015).
[40] J. Shi, L. Yang, and C. D. Bain, Drying of ethanol/water droplets containing silica nanoparticles, ACS Applied Materials & Interfaces **11**, 14275 (2019).
[41] Y. Li, C. Diddens, T. Segers, H. Wijshoff, M. Versluis, and D. Lohse, Evaporating droplets on oil-wetted surfaces: Suppression of the coffee-stain effect, Proceedings of the National Academy of Sciences **117**, 16756 (2020).
[42] R. G. Picknett and R. Bexon, The evaporation of sessile or pendant drops in still air, Journal of Colloid and Interface Science **61**, 336 (1977).
[43] R. V. Craster, O. K. Matar, and K. Sefiane, Pinning, retraction, and terracing of evaporating droplets containing nanoparticles, Langmuir **25**, 3601 (2009).
[44] K. L. Maki and S. Kumar, Fast evaporation of spreading droplets of colloidal suspensions, Langmuir **27**, 11347

(2011).
[45] J. M. Stauber, S. K. Wilson, B. R. Duffy, and K. Sefiane, On the lifetimes of evaporating droplets, Journal of Fluid Mechanics **744**, R2 (2014).
[46] T. Pham and S. Kumar, Drying of droplets of colloidal suspensions on rough substrates, Langmuir **33**, 10061 (2017).
[47] G. Hu, J. Kang, L. W. T. Ng, X. Zhu, R. C. T. Howe, C. G. Jones, M. C. Hersam, and T. Hasan, Functional inks and printing of two-dimensional materials, Chem. Soc. Rev. **47**, 3265 (2018).
[48] C. Poulard and P. Damman, Control of spreading and drying of a polymer solution from Marangoni flows, Europhysics Letters (EPL) **80**, 64001 (2007).
[49] D. Bonn, J. Eggers, J. Indekeu, J. Meunier, and E. Rolley, Wetting and spreading, Rev. Mod. Phys. **81**, 739 (2009).
[50] D. Orejon, K. Sefiane, and M. E. R. Shanahan, Stick–slip of evaporating droplets: Substrate hydrophobicity and nanoparticle concentration, Langmuir **27**, 12834 (2011).
[51] B. M. Weon and J. H. Je, Self-pinning by colloids confined at a contact line, Phys. Rev. Lett. **110**, 028303 (2013).
[52] M. Kuang, L. Wang, and Y. Song, Controllable printing droplets for high-resolution patterns, Advanced Materials **26**, 6950 (2014).
[53] L. Keiser, H. Bense, P. Colinet, J. Bico, and E. Reyssat, Marangoni bursting: Evaporation-induced emulsification of binary mixtures on a liquid layer, Phys. Rev. Lett. **118**, 074504 (2017).
[54] Y. Li, P. Lv, C. Diddens, H. Tan, H. Wijshoff, M. Versluis, and D. Lohse, Evaporation-triggered segregation of sessile binary droplets, Phys. Rev. Lett. **120**, 224501 (2018).
[55] A. P. Mouat, C. E. Wood, J. E. Pye, and J. C. Burton, Tuning contact line dynamics and deposition patterns in volatile liquid mixtures, Phys. Rev. Lett. **124**, 064502 (2020).
[56] Y. L. Kong, I. A. Tamargo, H. Kim, B. N. Johnson, M. K. Gupta, T.-W. Koh, H.-A. Chin, D. A. Steingart, B. P. Rand, and M. C. McAlpine, 3d printed quantum dot light-emitting diodes, Nano Letters **14**, 7017 (2014).
[57] N. J. Cira, A. Benusiglio, and M. Prakash, Vapour-mediated sensing and motility in two-component droplets, Nature **519**, 446 (2015).
[58] R. Malinowski, I. P. Parkin, and G. Volpe, Advances towards programmable droplet transport on solid surfaces and its applications, Chem. Soc. Rev. **49**, 7879 (2020).
[59] H. N. Yow and S. Biggs, Probing the stability of sterically stabilized polystyrene particles by centrifugal sedimentation, Soft Matter **9**, 10031 (2013).
[60] C. L. Yaws, ed., *Chemical Properties Handbook* (McGraw-Hill, 1999).
[61] G. A. Lugg, Diffusion coefficients of some organic and other vapors in air, Analytical Chemistry **40**, 1072 (1968).
[62] J. J. Jasper, The surface tension of pure liquid compounds, Journal of Physical and Chemical Reference Data **1**, 841 (1972).
[63] W. M. Haynes, ed., *CRC Handbook of Chemistry and Physics*, Vol. 95 (CRC press, 2014).
[64] H. El-Kashef, The necessary requirements imposed on polar dielectric laser dye solvents, Physica B: Condensed Matter **279**, 295 (2000).
[65] I. Z. Kozma, P. Krok, and E. Riedle, Direct measurement of the group-velocity mismatch and derivation of the refractive-index dispersion for a variety of solvents in the ultraviolet, J. Opt. Soc. Am. B **22**, 1479 (2005).
[66] E. L. Talbot, L. Yang, A. Berson, and C. D. Bain, Control of the particle distribution in inkjet printing through an evaporation-driven sol–gel transition, ACS Applied Materials & Interfaces **6**, 9572 (2014).
[67] J. C. R. Reis, I. M. S. Lampreia, Â. F. S. Santos, M. L. C. J. Moita, and G. Douhéret, Refractive index of liquid mixtures: Theory and experiment, ChemPhysChem **11**, 3722 (2010).
[68] J. N. Israelachvili, *Intermolecular and Surface Forces* (Academic press, 2011).
[69] W. D. Ristenpart, P. G. Kim, C. Domingues, J. Wan, and H. A. Stone, Influence of substrate conductivity on circulation reversal in evaporating drops, Phys. Rev. Lett. **99**, 234502 (2007).
[70] Y. O. Popov, Evaporative deposition patterns: Spatial dimensions of the deposit, Phys. Rev. E **71**, 036313 (2005).
[71] K. B. Glasner and T. P. Witelski, Coarsening dynamics of dewetting films, Phys. Rev. E **67**, 016302 (2003).
[72] A. A. Pahlavan, L. Cueto-Felgueroso, A. E. Hosoi, G. H. McKinley, and R. Juanes, Thin films in partial wetting: stability, dewetting and coarsening, Journal of Fluid Mechanics **845**, 642 (2018).
[73] J. Eggers and L. M. Pismen, Nonlocal description of evaporating drops, Physics of Fluids **22**, 112101 (2010).